D5.3 Reports of results of the implemented DApOS

Deliverable Lead	Arpap for the DApOAS
Deliverable due date	2023/01/31
Status	FINAL
Version	V1.0

Co-financed by the Connecting Europe Facility of the European Union

DOCUMENT CONTROL PAGE

Title	D5.3
Creator	Arpap
Publisher	Highlander Consortium
Contributors	Simona Barbarino (ARPAP), Nicola Loglisci (ARPAP)
Type	Report
Language	EN
Rights	Copyright “Highlander Consortium”
Audience	X Public
	Restricted
Requested deadline	M40

Index

1 Aim of the DApOS “Forest Fire Potential”

The aim of the DApOS “Forest Fire Potential” is to provide mid-term projections of forest fire potential over the Piedmont Region. To reach this aim, the calculation of the Fire Weather Index System (hereafter FWI), which expresses an exhaustive description of fire behaviour and spread, starting from meteorological conditions, is carried out .

This DApOS describes the analysis of forest fire potential comparison between the reference period (1991-2020) and the near future period (2021-2050) of the main components of FWI. Such examination is carried out by using the Very High-Resolution Climate datasets developed by CMCC.

2 Data and Methods

2.1 Very High-Resolution climate datasets

Highlander Very High-Resolution Projections (VHR-PRO) is a downscaling, by means of COSMO-CLM, of the COSMO-CLM simulation over Italy at 8 km horizontal resolution (Bucchignani et al., 2016), in turn, driven by the Global Climate Model CMCC-CM (Scoccimarro et al., 2011), covering the time window 1989-2080 under the historical (1989-2005) and RCP 8.5 (2006-2050) scenarios. The downscaling, performed by CMCC, provides data with a horizontal resolution of about 2.2 km.

According to the 5th Assessment Report of IPCC (IPCC, 2014), RCP 8.5 is a Representative Concentration Pathway assuming a trajectory for atmospheric greenhouse gas concentration which leads to a radiative forcing of +8.5 W/m^2 by the end of the Century. RCP 8.5 is often defined as "the worst-case scenario" because such an increase in the radiative flux is only possible if no (or ineffective) mitigation strategies are adopted.

The temporal coverage of VHR-PRO can be divided into the reference period 1989-2005, – here labelled as VHR-PRO-HIST – and the near future 2006-2050, indicated as VHR-PRO-RCP8.5.

The dataset used as a benchmark to compare the future 2021-2050 VHR-PRO RCP8.5 is a downscaled ERA5 obtained using COSMO-CLM – here labelled VHR-REA. The horizontal spatial resolution is 2.2 km, as for the VHR-PRO simulations and the considered time range is 1991-2020, like the other case studies.

2.2 Fire Weather Index

The Fire Weather Index (FWI) (Van Wagner, 1987) is a meteorologically based index used worldwide to estimate fire danger. It consists of different components that account for the effects of fuel moisture and wind on fire behaviour and spread. The higher the FWI is, the more favorable the meteorological conditions to trigger a wildfire are [https://climate.copernicus.eu/fire-weather-index]

The Canadian Forest Fire Weather Index (FWI) System consists of six components. The first three components are fuel moisture codes, which are numeric ratings of the moisture content of the forest floor and other dead organic matter. Their values rise as the moisture content decreases. There is one fuel moisture code for each of the three layers of fuel: litter and other

fine fuels; loosely compacted organic layers of moderate depth; and deep, compact organic layers. The remaining three components are fire behaviour indices, which represent the rate of fire spread, the fuel available for combustion, and the frontal fire intensity; these three values rise as the fire danger increases [https://cwfis.cfs.nrcan.gc.ca/background/summary/fwi].

The diagram below illustrates the components of the FWI System. The calculation of the components is based on consecutive daily observations of temperature, relative humidity, wind speed, and 24-hour precipitation. The six standard components provide numeric ratings of relative potential for wildland fire.

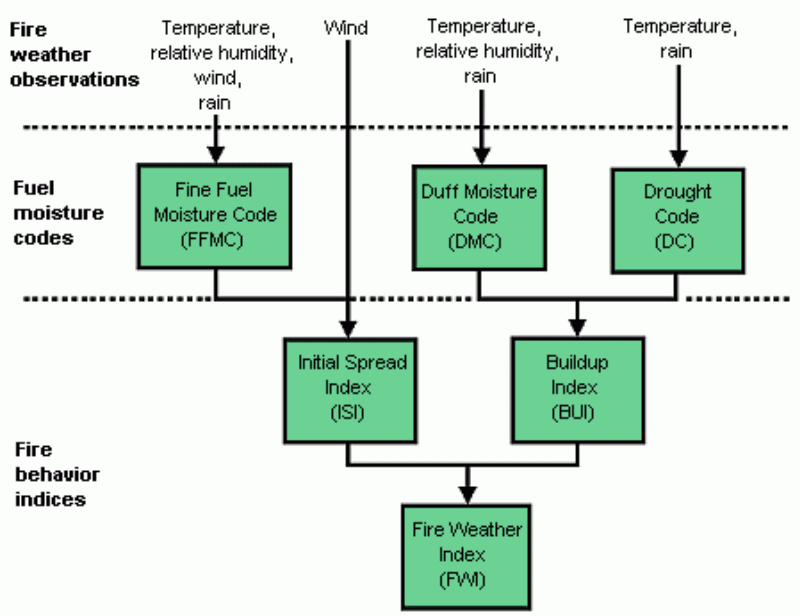

Figure 1. Diagram of Fire Weather Index [Van Wagner]

The Fine Fuel Moisture Code (FFMC) is a numeric rating of the moisture content of litter and other cured fine fuels. This code is an indicator of the relative ease of ignition and the flammability of fine fuel.

The Duff Moisture Code (DMC) is a numeric rating of the average moisture content of loosely compacted organic layers of moderate depth. This code indicates fuel consumption in moderate duff layers and medium-size woody material.

The Drought Code (DC) is a numeric rating of the average moisture content of deep, compact organic layers. This code is a useful indicator of seasonal drought effects on forest fuels and the amount of smoldering in deep duff layers and large logs.

The Initial Spread Index (ISI) is a numeric rating of the expected rate of fire spread. It is based on wind speed and FFMC. Like the rest of the FWI system components, ISI does not take fuel type into account. Actual spread rates vary between fuel types at the same ISI.

The Buildup Index (BUI) is a numeric rating of the total amount of fuel available for combustion. It is based on the DMC and the DC. The BUI is generally less than twice the DMC value, and moisture in the DMC layer is expected to help prevent burning in material deeper down in the available fuel.

The Fire Weather Index (FWI) is a numeric rating of fire intensity. It is based on the ISI and the BUI and is used as a general index of fire danger.
[https://cwfis.cfs.nrcan.gc.ca/background/summary/fwi]

2.3 Input data

The Fire Weather Index is calculated over three datasets: VHR-REA for the reference period (1991-2020), VHR-PRO-HIST (1989-2005) to be employed for a bias adjustment technique, and VHR-PRO-RCP 8.5 for the near future projections (2021-2050).

For all datasets employed, the input data are as follows:

- 2m temperature - instantaneous values at 12 pm UTC
- 10 m U, V wind - instantaneous values at 12 pm UTC. The U and V components are used for wind speed calculation.
- 2m dewpoint temperature – instantaneous values a 12 pm UTC. This variable is used, in combination with 12 pm UTC 2m temperature, for relative humidity evaluation.
- hourly precipitation.- It is needed to evaluate the total precipitation accumulated in a 24 hours time window starting from from 12 pm UTC of the previous day.

Direct model output coming from VHR-PRO projections has been post-processed to remove any systematic error, through a linear scaling technique (LS) of bias adjustment.

To this aim, VHR-PRO-HIST and VHR-ERA data were compared over the common period 1989-2005.

Linear scaling (LS) is the most straightforward bias correction technique employed in several studies (Ines et al. 2006; Teutschbein et al. 2013). LS method aims to perfectly match the monthly mean of corrected values with that of observed ones (Lenderink et al., 2007). It operates with monthly correction values based on the differences between observed and raw

data. On a monthly basis, precipitation is typically corrected with a multiplier; temperature is corrected with an additive term. [*Gunavathi et al., 2021*].

The relation used for the temperature field is as follows:

biasT = T_VHR_ERA – T_VHR-PRO-HIST

T_VHR-PRO_corrected = T_VHR-PRO + biasT

Instead, as far as precipitation data are concerned, the correction is applied as follows:

biasPr= Pr_VHR_ERA/Pr_VHR-PRO-HIST

Pr_VHR-PRO_corrected = Pr_VHR-PRO x biasPr

In this study we apply such bias adjustment technique to the whole dataset of input meteorological variables: wind speed is corrected with a multiplier, as precipitation field. The relative humidity is calculated from 2m temperature and dew point temperature 2m, both previously corrected with the additive term.

3 Results

The purpose of this DaPos is to provide a complete analysis of current and future forest fire potential in the Piedmont Region, through the comparison between the reference period (1991-2020) and the near future projections (2021-2050).

Our first and necessary intent is to investigate relative changes in mean and extreme conditions regarding the driving meteorological variables (temperature, wind speed, relative humidity, total precipitation), to better understand in which manner climate forcing is responsible for the resulting fire potential fluctuations.

Afterward, we focus on two indices of the FWI System, which describe the moisture content related to different fuel layers: Fine Fuel Moisture Code FFMC for the surface layer, and Drought Code DC for the deepest layer. These indexes are related to meteorological conditions to various scales, because of time-lag which spans from 2-3 days for FFMC to almost two months for DC [https://cwfis.cfs.nrcan.gc.ca/background/summary/fwi]. We also take into account the final Fire Weather Index FWI. As the indices are directly proportional to dangerous conditions, the higher the fire danger, the more dangerous the conditions.

We take into consideration the same types of evaluations both for reanalysis data and projections simulations. In particular, we integrate the analysis of median values with a focus on the highest percentiles of the distributions.

Here listed the complete analyses for each variable:

- Maps of probability of exceedance of the 50^{th},90^{th},95^{th} and 99^{th} percentiles
- Annual cycle of monthly values of the 50^{th},90^{th},95^{th} and 99^{th} percentiles
- Probability density function PDF
- Boxplots

For relative humidity and precipitation, we also explore the lowest values of distributions, through a focus on the 1^{st}, $5^{th,}$ and 10^{th} percentiles. In addition, as regards precipitation, we explore the three cases of consecutive dry days, days with precipitation in the range of 1-5mm, and days with precipitation in the range 5-10 mm.

We conduct the whole analysis over meteorological seasons (hereafter DJF, MAM, JJA, SON) to observe the variations of climate-forcing drivers. But we are also interested in the fire potential evaluation, more connected with changes during the vegetation cycle of forest types. For this aim, we divide our examination also between the non-vegetative season – which spans from December to April – and the vegetative season, from May to November.

The provided output of the DaPOS "Forest Fire Potential" are the values of FFMC, DC, and FWI for the reference (1991-2020) and projection (2021-2050) periods, expressed as statistical distribution (50^{th}, 90^{th}, 95^{th}, and 99^{th} percentiles). In particular, we provide the probability of exceedance of the 50th, 90^{th}, 95^{th}, and 99^{th} percentiles (extracted from the 1991-2020 distributions) in the projection distributions (2021-2050) over both meteorological (DJF, MAM, JJA, SON) and vegetative/non vegetative seasons.

3.1 Driving meteorological variables

Temperature

Regarding the results about temperature, future projections show a strong increase in monthly values between January and March and a slighter positive variation during July and August. Figure 2a shows a general shift towards higher values during the non-vegetative season, mainly related to the increase in the alpine montane belt. Such results are confirmed by the map of the probability of exceedance of the 50^{th} and 95^{th} percentile (figure 3a,3b).

During the vegetative season, the change involves the most of probability density function, also maxima values (figure 2b). Again, the alpine areas are mostly affected by an enhanced probability in the 50^{th}, 90^{th},95^{th}, and 99^{th} percentiles (not shown).

In particular, the probability of the 50^{th} percentile increases in the montane alpine belt, but it doesn't show a significant variation in plain areas. For the 90^{th} percentile, the biggest fluctuations occur again on the montane alpine belt, more and more moving from hills toward doubled values at the highest elevations. Over plains, projections do not change, keeping around 10%. Similar spatial patterns are evident from 95^{th} and 99^{th} percentiles maps (not shown).

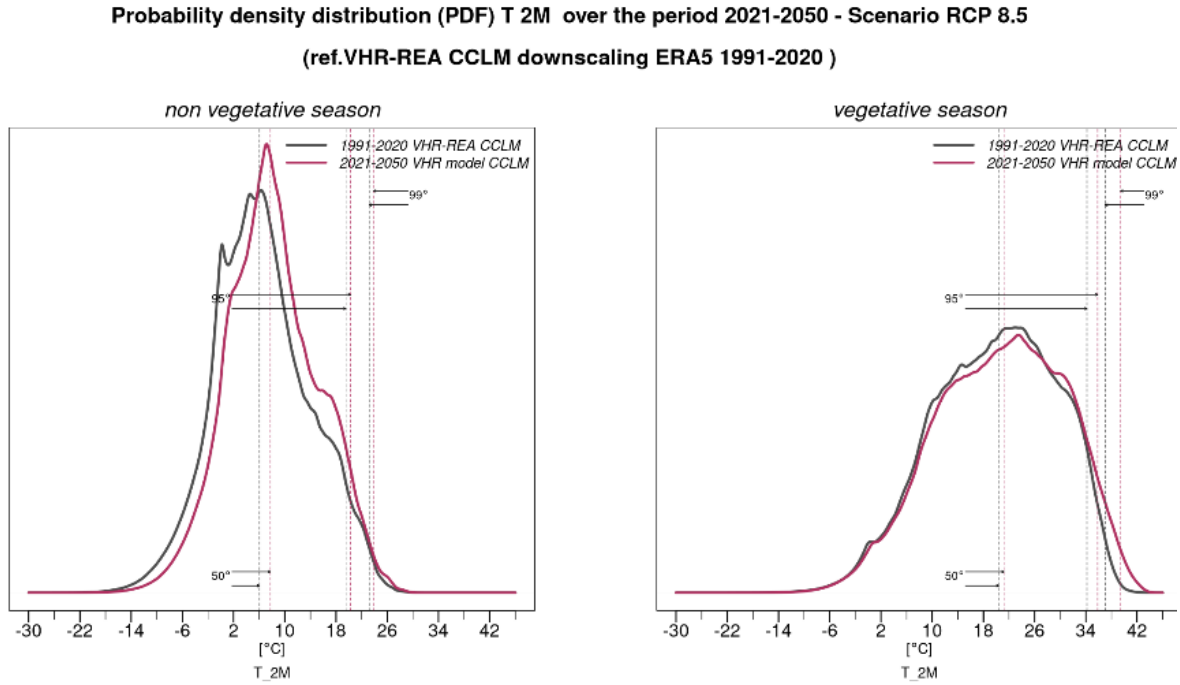

Figure 2. Probability density function (PDF) of 2m temperature –2021-2050 period (red line) and 1991-2020 period (grey line). Panels show non-vegetative seasons (figure 2a, on the left) and vegetative seasons (figure 2b, on the right).

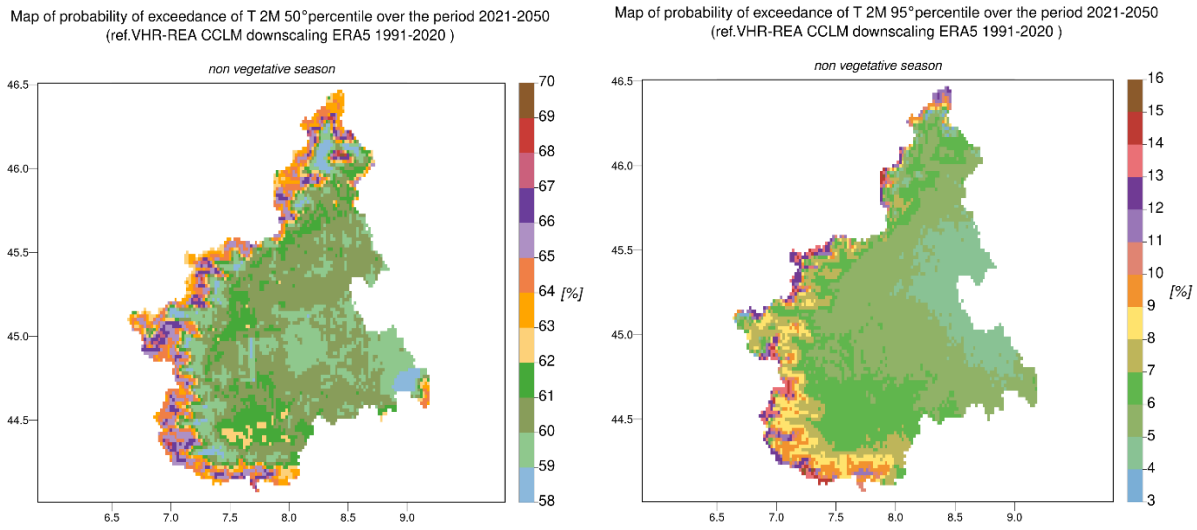

Figure 3. Map of exceedance probability of of the 50th (figure 3a, on the left) and 95th percentiles (figure 3b, on the right) extracted from the 1991-2020 temperature distributions, in the projection distributions (2021-2050). Panels show the analysis of non-vegetative season (Dec, Jan, Feb, Mar, Apr).

PRECIPITATION

Precipitation analysis shows the most interesting results, as regards diverse variations according to low, median, and high distribution values, with various spatial patterns related to land elevation.

As shown from the annual cycles of consecutive dry days, of the number of days in the range of 1-5 mm and of the number of days in the range of 5-10 mm (figure 4), during winter months (DJF) and March the decrease in the number of consecutive dry days is replaced by a slight increase in low precipitation values over the alpine montane belt (figure 5, left side); in contrast, winter projections in plains areas show a clear reduction, not only in low and median values but also of intense precipitation events.

During summer, a strong precipitation drop is evident over the entire region, associated to an increase in dry spells, more severe at lower altitudes. But, besides a general decrease in the low and mean percentiles (figure 5a, figure 5b), the highest percentiles projections show an increase in precipitation(figure 4), possibly connected to severe atmospheric instability and convective events.

During autumn the most remarkable result is the huge increase of the highest percentiles over plains areas but combined with a persistance of dry days along September.

Moreover, the precipitation regime shows a shift backwardof the autumn peak (figure 4, 90^{th}, 99^{th} percentiles), as the usual November maximum is moved up towards October.

Even if these are preliminary results, we could expect that in the future precipitation regime the autumn peak will occur earlier, than the regime characterizeing the Piedmont climate at present. The intensity of extreme events could be enhanced, by the strong increase in the probability of exceedance of the highest percentiles. Conditions at higher elevations seem to maintain values more similar to the current situation, both for median and extreme values.

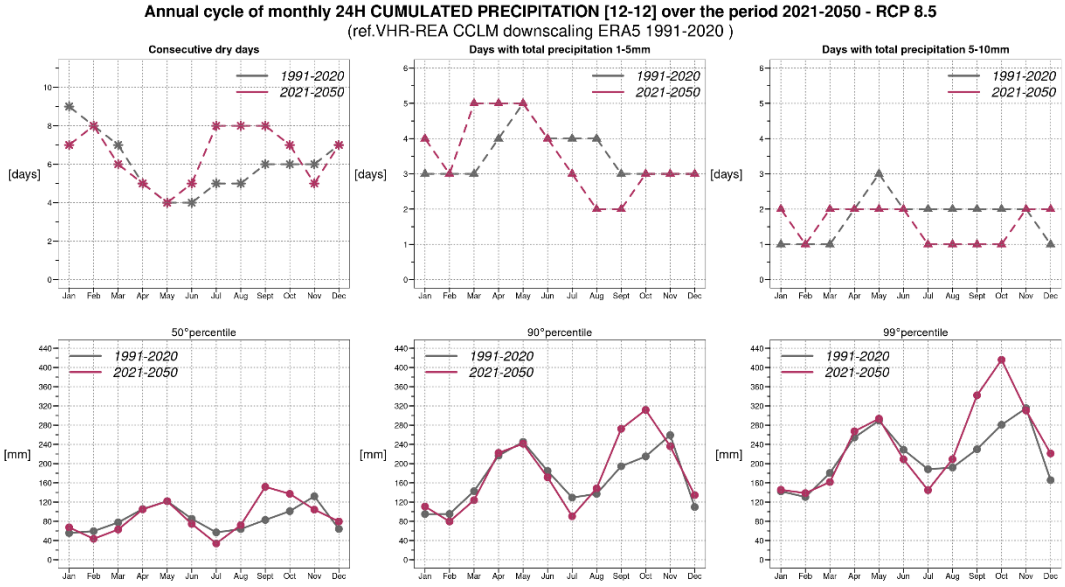

Figure 4. Annual cycle of monthly mean values related to precipitation regime. From left to right and from top to bottom: consecutive dry days, number of days in the range 1-5 mm and 5-10 mm, 50th, 90th, and 99th percentiles.

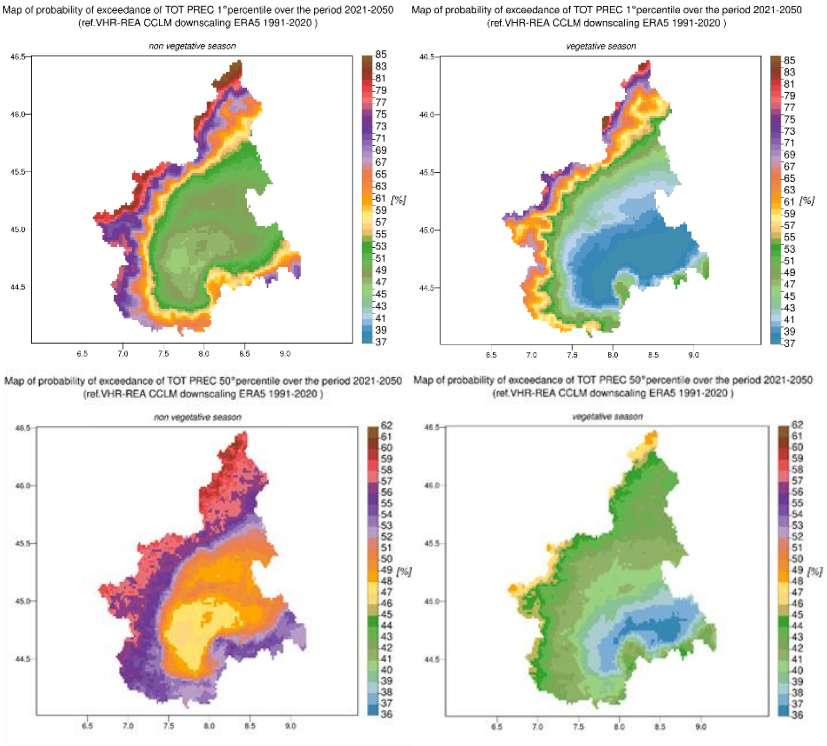

Figure 5: Map of exceedance probability of of the 10th percentile (figure 5a, top panel) and the 50th percentile (figure 5b, bottom panel), extracted from the 1991-2020 precipitation distributions, in the projection distributions (2021-2050). Panels show non-vegetative seasons on the left column and vegetative season on the right column.

RELATIVE HUMIDITY

As expected from the precipitation analysis, during the non-vegetative season we obtain a decrease of the highest percentiles of relative humidity in plains regions and a correspondent increase in low median values, due to the increased number of days with low or moderate precipitation, particularly over montane belt (not shown here). In summer a general decrease is confirmed, more pronounced over plains regions. During autumn is evident the strong fall around the highest percentile values, mostly over plains.

WIND SPEED

From monthly mean values of wind speed (figure 6), we can't notice evident changes in spring and summer, but a slight increase in extreme values is clear during winter and autumn.

Regarding winter, a reasonable, but a preliminary explanation, could be a more frequent occurrence of days characterized by zonal winds and föhn episodes, i.e. westerly synoptic configurations, which also could explain the increase of low precipitation values across the Alps and montane belt.

In autumn, the combination with an enhancement of extreme values of precipitation could be associated with more intense southwest fluxes and deep troughs over the Mediterranean Sea in more frequent "block" synoptic configurations, typical of autumn floods over Ligurian Gulf and South Piedmont areas.

During autumn, we notice the increase of the highest values occurs in combination with an enhancement of extreme values of precipitation. As autumn is the typical season of floods over Piedmont, from such preliminary results we can suppose a further increase of frequency of floods, associated with strong wind gusts

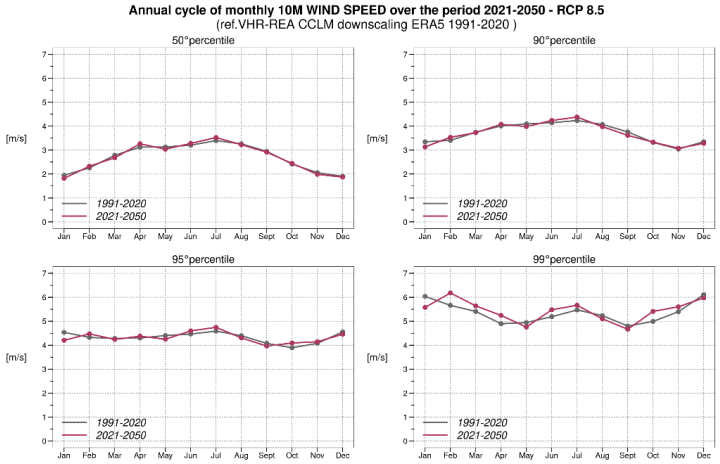

Figure 6. Annual cycle of monthly mean wind speed. From left to right: 50th, 90th, 95th,

99th percentiles.

In general, these first results about meteorological variables suggest an eventual change in precipitation regime from the end of summer until October and they need further deepening, also concerning potential modifications in synoptic configurations.

3.2 Forest fire potential

After a general description of the future climate context, we can better comprehend the projected fire potential variations.

Fine Fuel Moisture Code

Firstly, we take into consideration the Fine Fuel Moisture Code (FFMC), an indicator of the relative ease of ignition and the flammability of fine fuel. It expresses the status of surface fuel litter, connected with daily changes in meteorological conditions.

In general, we can't notice any significant change. From Figure 7a we observe slight positive variations during winter and a decrease in autumn, more evident from boxplots (figure 7b). During summer (figure 8) we expect some higher values - over mountain areas as regards the 50th percentiles and over west Piedmont for the 90th percentile values.

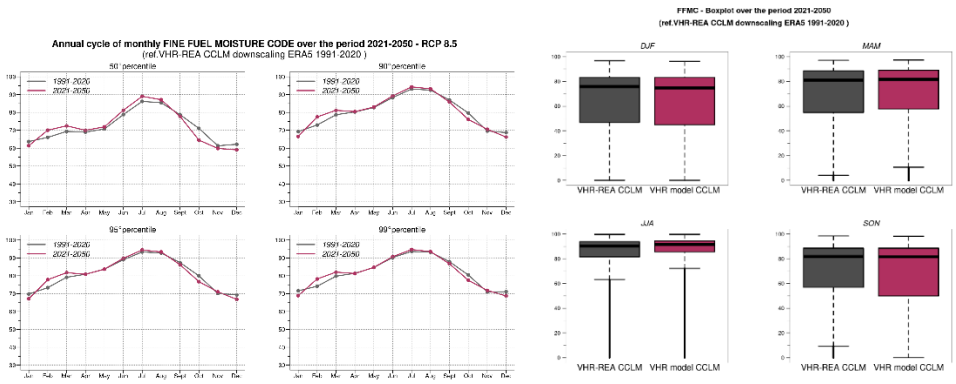

Figure 7. Left panel: the annual cycle of monthly mean values of FFMC. From left to right: 50th, 90th, 95th, and 99th percentiles. Right panel: FFMC boxplots, 2021-2050 period (red) with respect to 1991-2020 (grey). Panels show meteorological seasons: from top-left to bottom-right DJF, MAM, JJA, SON.

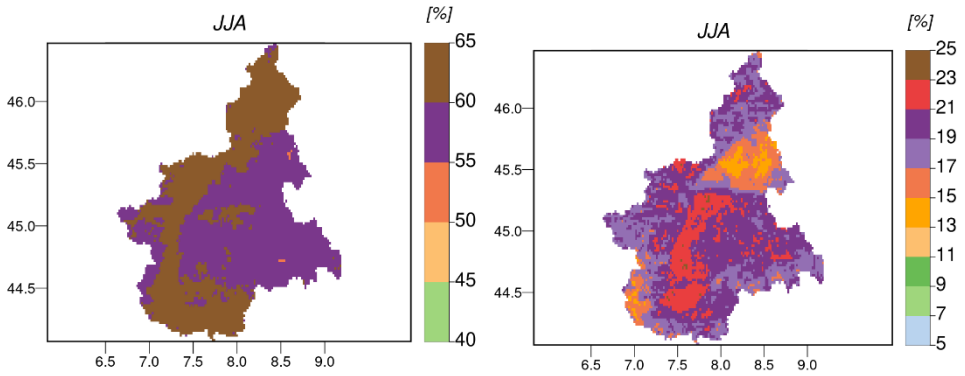

Figure 8: Map of exceedance probability of of the 50th percentile (figure 8a, left) and 90th percentile values (figure 8, right) extracted from the 1991-2020 FFMC distributions, in the projection distributions (2021-2050). Panels show summer season JJA.

Drought Code

Drought Code (DC) is a useful indicator of seasonal drought effects on forest fuels and the amount of smoldering in deep duff layers and large logs. Here we can appreciate a slight decrease in the upper part of the distribution during winter (figure 9a). A more pronounced variation is evident during summer and autumn, as shown in figure 9. Summary results can be well inferred by boxplots. They display a moderate decrease in autumn, from median to highest percentiles, due to a more intense precipitation regime. Also, summer variations are clear from the correspondent boxplots, which maintain the median values but enhance the upper part of the distribution.

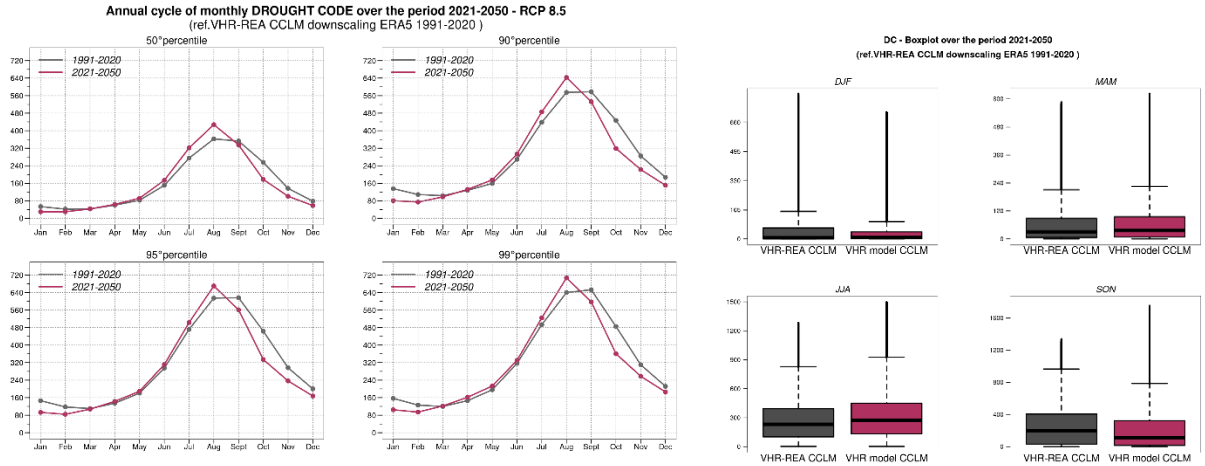

Figure 09. Left panel (figure 9a): the annual cycle of monthly mean values of DC. From left to right: 50th, 90th, 95th, and 99th percentiles. Right panel (figure 9b): DC boxplots in 2021-2050 period (red) with respect to 1991-2020 (grey). Panels show meteorological seasons from top-left to bottom-right DJF, MAM, JJA, SON.

Maps of the probability of exceedance of the 50th percentile (figure 10) allow displaying, for winter, almost stationary conditions over the Alps with some local slight increase, combined with a general decrease over plains. During summer, future longer dry spells explain the DC variations.

The probability of exceedance of the 50th percentile becomes 60-70% in almost the whole region. As expected, maps of the probability of exceedance of 95th percentiles (figure 11) show much stronger variations. The probability of exceedance rises from 5% to 10% over south Piedmont; a homogeneous greater increase in the range 10-15% is clear over plains; northern areas are affected by the worse result, the probability of exceedance reaching values equal or greater than 20% in the period 2021-2050.

A general decrease, as expected, is evident in autumn, with a quite uniform spatial pattern.

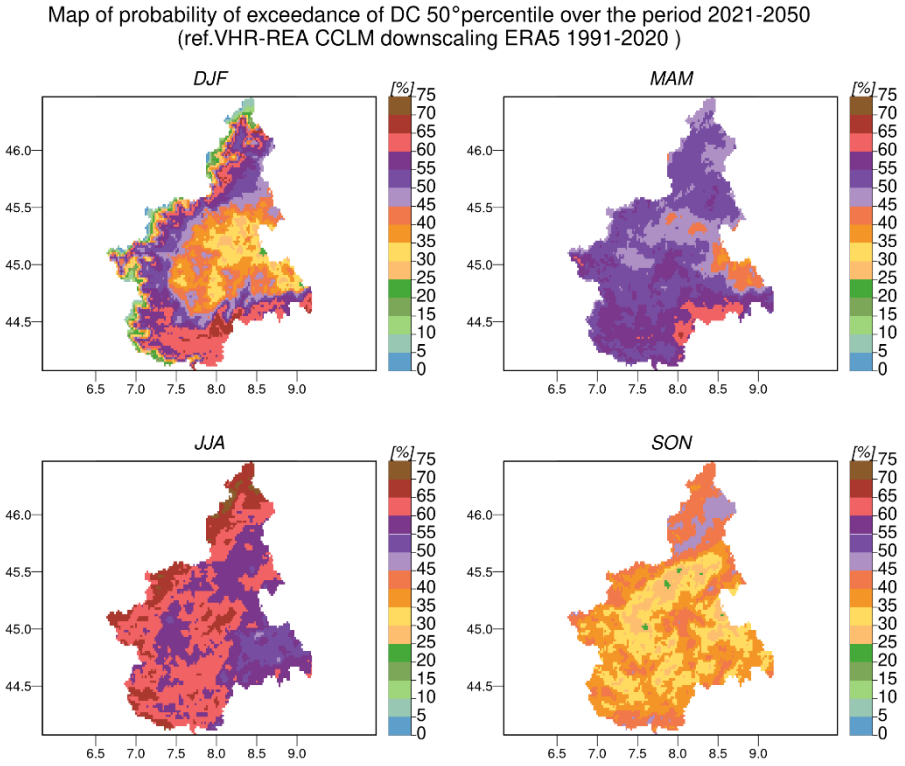

Figure 10: Map of exceedance probability of of the 50th percentile extracted from the 1991-2020 DC distributions, in the projection distributions (2021-2050) for DJF, MAM, JJA, SON (from top-left to bottom-right).

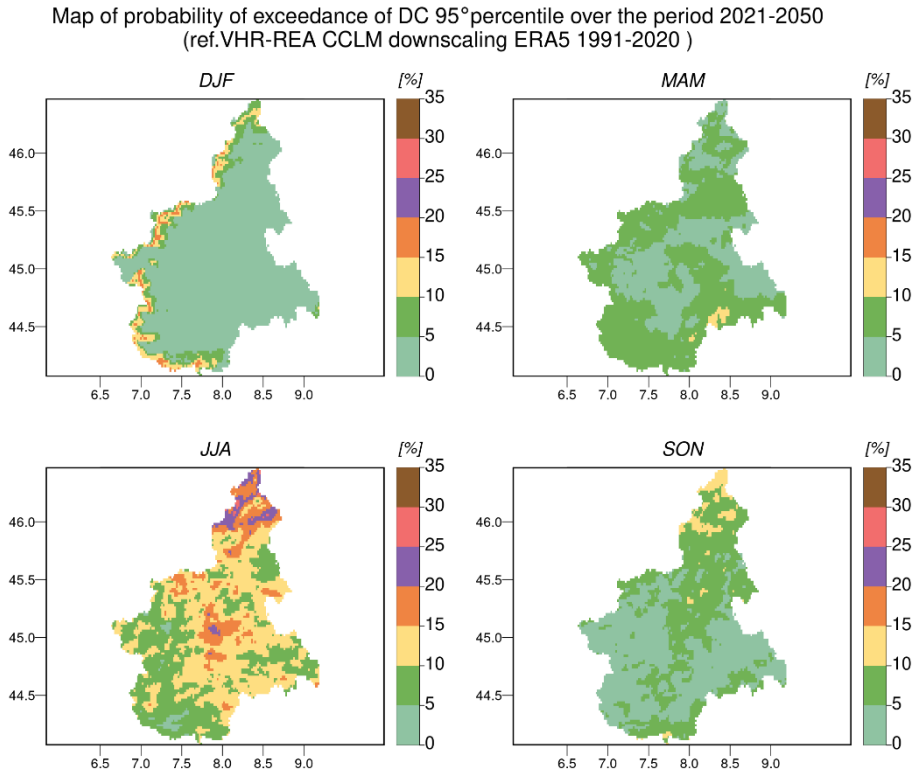

Figure 11: Map of exceedance probability of of the 95th percentile extracted from the 1991-2020 DC distributions, in the projection distributions (2021-2050) for DJF, MAM, JJA, SON (from top-left to bottom-right).

Fire Weather Index

At the end of our analysis, through the discussion on fire Weather Index results, we can comprehend the global variations of fire behaviour and spread, related to the complete description of fire danger conditions.

Monthly mean values of FWI (figure 12a), show a general increase throughout the year, except for December and January. The huge summer variations are explained by the strongly enhanced drought, which starts in spring and is more and more pronounced until the end of August. Maps show that plains are more involved in such an increase, but also the montane alpine belt is affected by a strong rise in the probability of exceedance of the 50th and 90th percentiles in the period 2021-2050 (figure 13-14). In particular, the 90th percentile reaches the probability of exceedance of 60-70% in alpine valleys. Boxplots confirm such an increase during the hottest months.

During winter t a slight decrease is observed at high elevations, due to the decrease of consecutive dry days in those areas. An increase is evident over plains, due to less precipitation amount in low and moderate daily ranges.

Boxplots and maps help to reveal in which manner the distributions will be affected also during autumn, with median values and high percentiles in slightly decreasing over alpine areas, but moderately increasing over plains although more intense precipitation events, due to a rise in consecutive dry days during September and an enhanced daily meteorological variability along this period of the year, in the future.

In spring, although not significant changes in climate conditions are not expected, the consequences of minor variations for each input variable are sufficient to explain the projected increase of overall fire danger conditions.

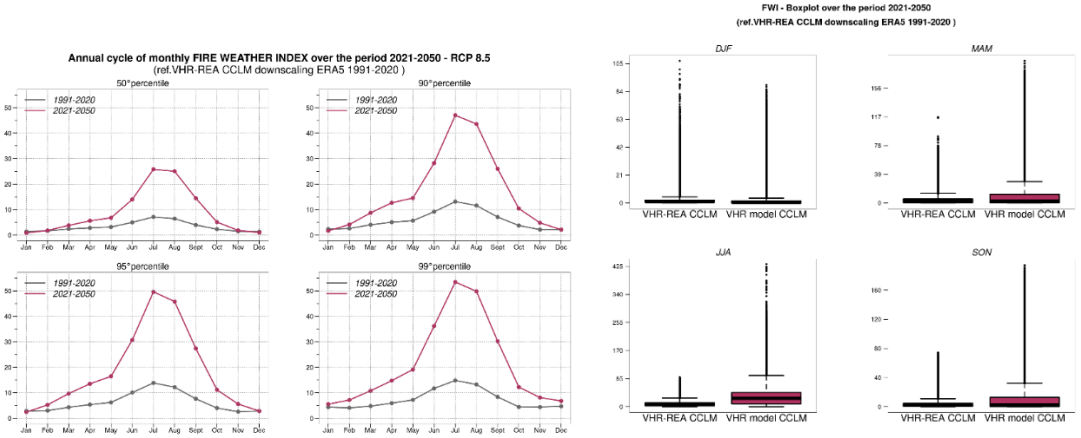

Figure 12. Left panel (figure 12a): the annual cycle of monthly mean values of FWI. From left to right: 50th, 90^{th,} 95th, and 99th percentiles. Right pane figure 12b): FWI boxplots, 2021-2050 period (on the right side) with respect to 1991-2020 (on the left side). Panels show meteorological seasons from top-left to bottom-right (DJF, MAM, JJA, SON).

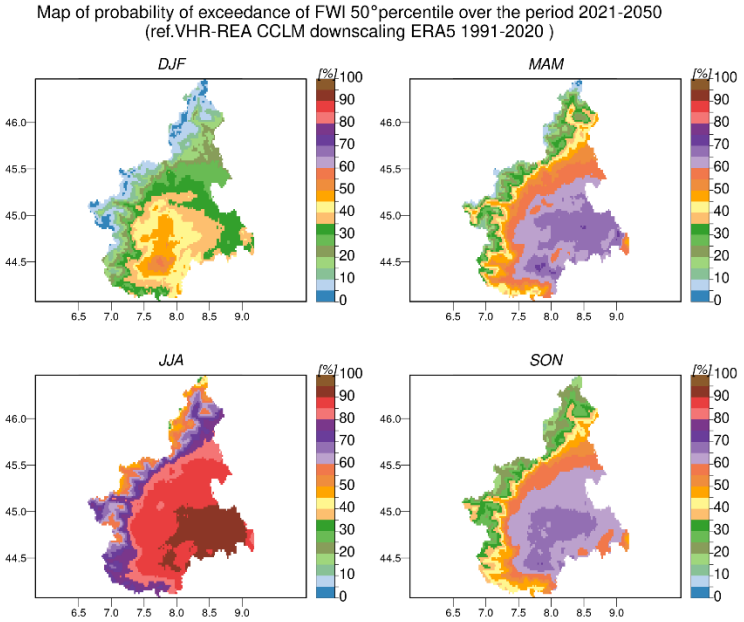

Figure 13: Map of exceedance probability of the 50th percentile extracted from the 1991-2020 FWI distributions, in the projection distributions (2021-2050) for DJF, MAM, JJA, SON (from top-left to bottom-right).

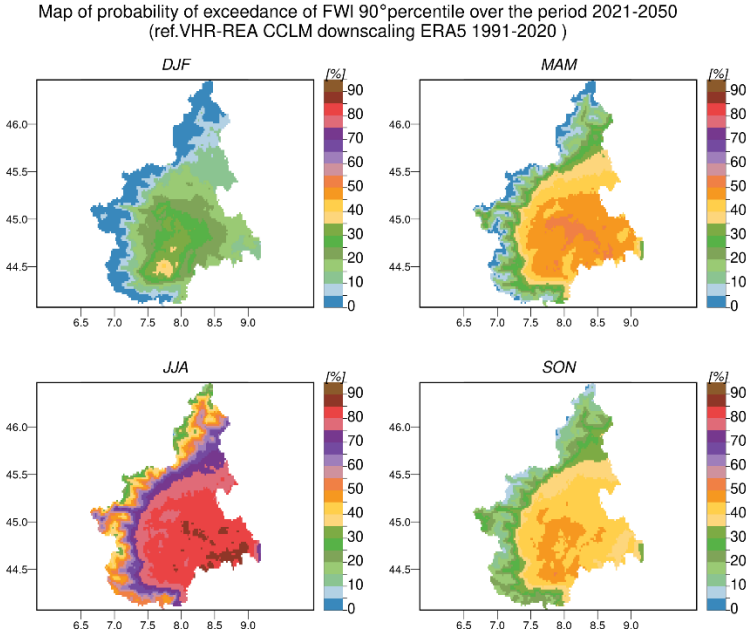

Figure 14: Map of the exceedance probability of the90th percentile extracted from the 1991-2020 FWI distributions, in the projection distributions (2021-2050) for DJF, MAM, JJA, SON (from top-left to bottom-right).

4 Conclusions

We conduct anassessment addressed to obtain a complete overview of forest fire potential changes in the near future 2021-2050, in comparison with the current conditions represented bythe reference period 1991-2020.

Here we focus on the montane alpine belt and elevations at which forests can develop, so our interest is mainly addressed to valleys and slightly higher elevation areas.

During cold months we expect a general decrease in fire danger conditions, but a wider climate variability could result in an increase of few days affected by severe fire potential.

The worst conditions will occur during summer, due to a large increase of drought and temperature, not only over plains, but also at high elevations.

During spring we expect a slight increase in fire danger conditions because, despite of the small variations in climate-forcing variables, the fluctuations of predisposing factors can concur to generate suitable conditions for the worsening of forest fire potential.

Results are heterogeneous for the different components of the FWI system, related to different fuel layers.

FFMC projections are different from DC results, thanks to the skill of the model to reproduce diverse precipitation regimes, both advective fluxes, and strong instability conditions.

Such definite results in different ranges of probability distributions, as detailed spatial patterns moving from plains to mountain areas, are enabled by the employment of the state-of-the-art very high-resolution model VHR-PRO COSMO-CLM, which can better describe not only complex topography as in the case of Piedmont region, but also the interaction between fluxes and alpine areas and physical processes such as convection.

Further investigations are necessary. It could be of some interest to explore future synoptic configuration modifications, as it could be worth applying more sophisticated bias-adjustment techniques tailored for the tails of probability density distributions, in order to improve the preliminary results presented in this report.

REFERENCES

Bucchignani, E., Montesarchio, M., Zollo, A.L. & Mercogliano, P. (2016). High-resolution climate simulations with COSMO-CLM over Italy: performance evaluation and climate projections for the 21st century. International Journal of Climatology 36(2), 735-756.

Gunavathi, S., and R. Selvasidhu. "Assessment of Various Bias Correction Methods on Precipitation of Regional Climate Model and Future Projection." (2021).

Ines, Amor VM, and James W. Hansen. "Bias correction of daily GCM rainfall for crop simulation studies." Agricultural and forest meteorology 138.1-4 (2006): 44-53.

IPCC, 2014. Climate Change 2014: Synthesis Report. Contribution of Working Groups I, II and III to the Fifth Assessment Report of the Intergovernmental Panel on Climate Change [Core Writing Team, R.K. Pachauri and L.A. Meyer (eds.)]. IPCC, Geneva, Switzerland, 151 pp.

IPCC. 2013. Climate Change 2013: The Physical Science Basis. Contribution of Working Group I to the Fifth Assessment Report of the Intergovernmental Panel on Climate Change [Stocker, T.F., D. Qin, G.-K. Plattner, M. Tignor, S.K. Allen, J. Boschung, A. Nauels, Y. Xia, V. Bex and P.M. Midgley (eds.)]. Cambridge University Press, Cambridge, United Kingdom and New York, NY, USA, 1535 pp.

Lenderink, G., van Ulden, A., van den Hurk, B. et al. A study on combining global and regional climate model results for generating climate scenarios of temperature and precipitation for the Netherlands. Clim Dyn 29, 157–176 (2007).

Scoccimarro E., Gualdi, S., Bellucci, A., Sanna, A., Fogli, P.G., Manzini, E., et al. (2011). Effects of tropical cyclones on ocean heat transport in a high resolution coupled General Circulation Model. Journal of Climate 24, 4368-4384.

Teutschbein, C. and Seibert, J.: Is bias correction of regional climate model (RCM) simulations possible for non-stationary conditions?, Hydrol. Earth Syst. Sci., 17, 5061–5077, https://doi.org/10.5194/hess-17-5061-2013, 2013.

Van Wagner, C.E. (1987). Development and Structure of the Canadian Forest Fire Weather Index System, Canadian Forestry Service Forestry Technical Report 35, Ottawa.